

5-2017

## **Disease Modeling Using Fractional Differential Equations and Estimation**

Daniel P. Medina  
*The University of Texas Rio Grande Valley*

Follow this and additional works at: <https://scholarworks.utrgv.edu/etd>



Part of the [Mathematics Commons](#)

---

### **Recommended Citation**

Medina, Daniel P., "Disease Modeling Using Fractional Differential Equations and Estimation" (2017).  
*Theses and Dissertations*. 199.  
<https://scholarworks.utrgv.edu/etd/199>

This Thesis is brought to you for free and open access by ScholarWorks @ UTRGV. It has been accepted for inclusion in Theses and Dissertations by an authorized administrator of ScholarWorks @ UTRGV. For more information, please contact [justin.white@utrgv.edu](mailto:justin.white@utrgv.edu), [william.flores01@utrgv.edu](mailto:william.flores01@utrgv.edu).

DISEASE MODELING USING FRACTIONAL  
DIFFERENTIAL EQUATIONS AND  
ESTIMATION

A Thesis

by

DANIEL P. MEDINA

Submitted to the Graduate College of  
The University of Texas Rio Grande Valley  
In partial fulfillment of the requirements for the degree of

MASTER OF SCIENCE

May 2017

Major Subject: Mathematics



DISEASE MODELING USING FRACTIONAL  
DIFFERENTIAL EQUATIONS AND  
ESTIMATION

A Thesis  
by  
DANIEL P. MEDINA

COMMITTEE MEMBERS

Dr. Tamer Oraby  
Chair of Committee

Dr. Andras Balogh  
Committee Member

Dr. Erwin Suazo  
Committee Member

Dr. George Yanev  
Committee Member

May 2017



Copyright 2017 Daniel P. Medina

All Rights Reserved



## ABSTRACT

Medina, Daniel P., Disease Modeling using Fractional Differential Equations and Estimation. Master of Science (MS), May, 2017, 44 pp., 2 tables, 18 figures, references, 8 titles.

Ordinary differential equations has been the most conventional approach when modeling spread of infectious diseases. Effective research has shown that using fractional-order differentiation can be a very useful and efficient extension for some mathematical models. In this thesis, fractional calculus is used to depict an SEIR model with a system of fractional-order differential equations. I also simulate the fractional-order SEIR using integer-order numerical methods. I also establish the estimation framework and show that it is accurately working.



## DEDICATION

To my father, mother, brother, and girlfriend for all supporting me every step of the way.



## ACKNOWLEDGMENTS

I am extremely grateful and thankful towards my thesis advisor Dr. Tamer Oraby for all his help and guidance through my graduate program. Thank you to my committee, Drs. Andras Balogh, Erwin Suazo, and George Yanev, for their help through this process as well. Working together with my colleagues helped immensely through my graduate career as well. Lastly, the biggest influence throughout my academic career and biggest help at any time in need; I am indebted to my brother David Medina for his endless contribution to my learning and success.



## TABLE OF CONTENTS

	Page
ABSTRACT .....	iii
DEDICATION .....	iv
ACKNOWLEDGMENTS .....	v
TABLE OF CONTENTS .....	vi
LIST OF TABLES .....	viii
LIST OF FIGURES .....	ix
CHAPTER I. INTRODUCTION .....	1
1.1 Special Functions .....	1
1.1.1 Gamma Function .....	1
1.1.2 The Mittag-Leffler Function .....	2
1.2 Fractional Calculus and Differential Equations .....	3
1.2.1 The Caputo Derivative .....	4
1.3 Laplace Transform .....	7
1.3.1 Laplace Transform Examples .....	7
1.3.2 Inverse Laplace Transform .....	8
1.4 Algorithm .....	11
1.4.1 Examples of Fractional Differential Equations .....	11
1.5 Geometrical Interpretation of Fractional Integration .....	15
1.5.1 Left-sided Riemann-Liouville fractional integral .....	16
1.5.2 Right-sided Riemann-Liouville fractional integral .....	17
CHAPTER II. EPIDEMIOLOGICAL MODELS .....	21
2.1 SEIR Model .....	21
2.2 Stability Analysis of a Disease-Free Equilibrium .....	25
CHAPTER III. SIMULATIONS AND ESTIMATION .....	27
3.1 Estimation: Nonlinear Least Squares Method .....	31
3.2 Akaike Information Criterion .....	31

3.3 Results . . . . .	32
3.4 Data . . . . .	35
CHAPTER IV. CONCLUSION AND FUTURE WORK . . . . .	37
APPENDIX A . . . . .	38
BIBLIOGRAPHY . . . . .	43
BIOGRAPHICAL SKETCH . . . . .	44

## LIST OF TABLES

	Page
Table 1.1 Laplace Transform Examples . . . . .	7
Table 3.1 Estimated Results . . . . .	33



## LIST OF FIGURES

		Page
Figure 1.1	The Gamma function $\Gamma(x)$ . . . . .	2
Figure 1.2	The Mittag-Leffler function at $\alpha = 1, 2$ and $\beta = 1, 2$ [5]. . . . .	3
Figure 1.3	Graph of the actual solution compared to the estimate and the error. . . . .	13
Figure 1.4	The fence and its shadows: $I_t^1 f(t)$ and $I_t^\alpha f(t)$ , for $\alpha = \frac{3}{4}$ , $f(t) = t + \frac{\sin(t)}{2}$ [8].	18
Figure 1.5	The process of change of the fence's basis shape for $I_t^\alpha f(t)$ , $\alpha = \frac{3}{4}$ [8]. . . . .	19
Figure 1.6	Snapshots of the changing shadow of a changing fence for $I_t^\alpha f(t)$ , $\alpha = \frac{3}{4}$ , $f(t) = t + \frac{\sin(t)}{2}$ , with time interval $\Delta t = \frac{1}{2}$ between the snapshots [8]. . . . .	19
Figure 1.7	The process of change of the fence's basis shape for ${}_t I_{10}^\alpha f(t)$ , $\alpha = \frac{3}{4}$ [8]. . . . .	20
Figure 2.1	This model displays the compartmental flow of the SEIR model. . . . .	22
Figure 3.1	Graph of the SIR model and SEIR model using $\alpha = \frac{1}{2}$ and $\beta = 40$ . . . . .	27
Figure 3.2	Numerical solution of I when $\beta^\alpha = 5$ for different values of $\alpha$ . . . . .	28
Figure 3.3	Numerical solution of I when $\beta^\alpha = 10$ for different values of $\alpha$ . . . . .	28
Figure 3.4	Numerical solution of I when $\beta^\alpha = 20$ for different values of $\alpha$ . . . . .	29
Figure 3.5	Numerical solution of I when $\beta^\alpha = 40$ for different values of $\alpha$ . . . . .	29
Figure 3.6	Numerical solution of I when $\beta^\alpha = 0.5$ and $R_0 < 1$ for different values of $\alpha$ . . . . .	30
Figure 3.7	Side by side comparison of the model when $\alpha = .1$ and $\beta^\alpha = .5$ . . . . .	33
Figure 3.8	Side by side comparison of the model when $\alpha = .1$ and $\beta^\alpha = 30$ . . . . .	34
Figure 3.9	Side by side comparison of the model when $\alpha = .5$ and $\beta^\alpha = 30$ . . . . .	34
Figure 3.10	Side by side comparison of the model when $\alpha = .5$ and $\beta^\alpha = 40$ . . . . .	34



## CHAPTER I

### INTRODUCTION

Disease modeling has had an increasing number of approaches. Epidemiology is studied to further understand and estimate disease spread and control. For a long time, integer order differential models were used to depict disease models. With the increase of interest in fractional calculus, more fields have begun using this for several fields of research. Being able to use fractional calculus allows models to take into consideration the memory effect in the model. For each different disease, there exists a more suitable model to be used. In this thesis the SEIR model is used to show the transition between those who are susceptible, exposed, infected, and finally recovered. Depending on the disease of interest, different models are used. The different models and their specific applications are covered on Chapter 2.

#### 1.1 Special Functions

Since this thesis revolves around fractional calculus, it is important to also introduce some special functions that are used in this subject. Functions like the gamma, beta, and Mittag-Leffler functions are to be used in fractional calculus.

##### 1.1.1 Gamma Function

The Gamma function, denoted by  $\Gamma(z)$ , is a generalization of the factorial function when  $z$  is not an integer. Particularly,  $\Gamma(n) = (n - 1)!$  for  $n \in \mathbb{N}$ . For  $z > 0$ , it is defined as [5],

$$\Gamma(z) = \int_0^{\infty} t^{z-1} e^{-t} dt.$$

Some noteworthy examples of the Gamma function are:

$$\begin{aligned}
\Gamma(1) &= 1, \\
\Gamma(z+1) &= z\Gamma(z), \\
\Gamma\left(\frac{1}{2}\right) &= \sqrt{\pi}.
\end{aligned} \tag{1.1}$$

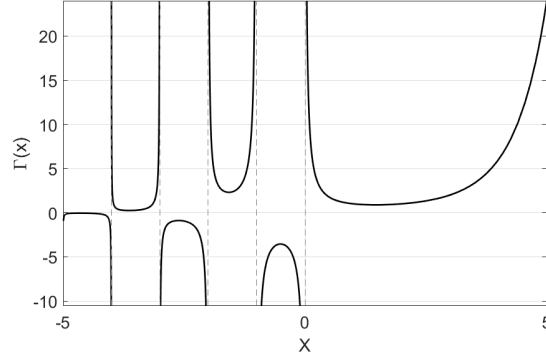


Figure 1.1: The Gamma function  $\Gamma(x)$ .

### 1.1.2 The Mittag-Leffler Function

The Mittag-Leffler is a function that generalizes the exponential function. The function can be written as follows[5],

$$E_{\alpha}(z) = \sum_{k=0}^{\infty} \frac{z^k}{\Gamma(\alpha k + 1)}, \quad \alpha \in \mathbb{R}^+, \quad z \in \mathbb{C}, \tag{1.2}$$

or more generally using two parameters,

$$E_{\alpha,\beta}(z) = \sum_{k=0}^{\infty} \frac{z^k}{\Gamma(\alpha k + \beta)}, \quad \alpha, \beta \in \mathbb{R}^+, \quad z \in \mathbb{C}. \tag{1.3}$$

**Note.** [4] Let  $\alpha, \beta > 0$  and  $z \in \mathbb{C}$ , and the Mittag-Leffler functions satisfy the equality given by Theorem 4.2 in [3],

$$E_{\alpha,\beta}(z) = zE_{\alpha,\alpha+\beta}(z) + \frac{1}{\Gamma(\beta)}. \tag{1.4}$$

Some interesting examples of the Mittag-Leffler function with  $\alpha = 0, 1, 2$  are [5]:

$$\begin{aligned}
E_{\alpha,1}(z) &= E_{\alpha}(z), \\
E_{0,1}(z) &= \frac{1}{1-z}; \text{ if } |z| < 1, \\
E_{1,1}(z) &= e^z, \\
E_{2,1}(z) &= \cosh(z), \\
E_{2,2}(z) &= \frac{\sinh(z)}{z}.
\end{aligned} \tag{1.5}$$

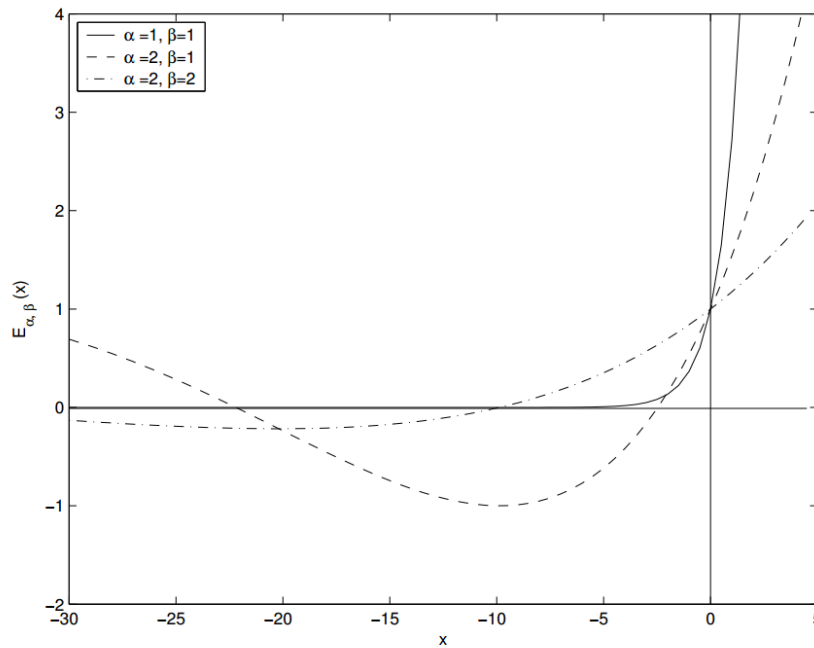


Figure 1.2: The Mittag-Leffler function at  $\alpha = 1, 2$  and  $\beta = 1, 2$  [5].

## 1.2 Fractional Calculus and Differential Equations

In 1675, Gottfried Leibniz achieved an amazing breakthrough by discovering differential and integral calculus. Since then, many mathematicians, namely Isaac Barrow, James Gregory, and Isaac Newton, explored this field even further. The concept of change in time through calculus has been a major part of mathematics since then. Such research opened up many fields of mathematics, like complex analysis, functional analysis, differential geometry, measure theory, and abstract algebra. In 1695 the idea of fractional calculus was sparked by L'Hopital and Leibniz; however, it

remained somewhat dormant until the past couple of decades when new fields of studies found this idea to be very useful. These two mathematicians sent letters to one another regarding the notation of differentiation of order  $\frac{1}{2}$  and its visual representation [7]. With the progression in the field of calculus, many other mathematicians have been contributors to this study like Laplace, Fourier, Abel, Liouville, Reimann, Grunwald, Letnikov, Heaviside, Weyl, Erdelyi, and even more [5]. From this, one might ask, "What makes fractional differentiation so important and different from integer-order differentiation?" The answer can be seen through comparing the effect both approaches have on the study. In medicine, finances or economics, physics, engineering, or describing polymers, arbitrary-ordered derivatives are extremely useful because of their added effect of memory and hereditary properties. These properties are not evident when using integer-order differentiation.

### 1.2.1 The Caputo Derivative

Through modification of the Riemann-Liouville derivative, the Caputo derivative was found with the goal of forming an extension from integer differential equations to fractional differential equation without the need to define fractional initial conditions. In this section,  $D^n$  will be used as the standard integer-order differential operator [5].

$$D^n f = \frac{d^n f}{dt^n} = f^{(n)}.$$

To show the following operators, we define  $J^n$  to be our integration operator of integer order given by,

$$J^n f(t) = \frac{1}{n!} \int_0^t (t - \tau)^{n-1} f(\tau) d\tau, \quad (1.6)$$

where  $n \in \mathbb{Z}^+$ . For fraction-order integrals, we use

$$J^{n-\alpha} f(t) = \frac{1}{\Gamma(n - \alpha + 1)} \int_0^t (t - \tau)^{n-\alpha-1} f(\tau) d\tau, \quad (1.7)$$

where  $n - 1 < \alpha \leq n$ .

**Remark 1.** *When using the integration operator for a fractional order  $n \in \mathbb{Q}$ .*

Thus, the representation for the Caputo fractional differential operator can now be defined as,

$$D_*^\alpha f(t) = J^{n-\alpha} D^n f(t),$$

where  $n - 1 < \alpha \leq n$ , for  $n \in \mathbb{N}$ .

We also introduce the Riemann-Liouville fractional derivative as,

$$D^\alpha f(t) = D^n J^{n-\alpha} f(t).$$

The Riemann-Liouville fractional derivative seems similar to the Caputo fractional operator but since

$$D^n J^{n-\alpha} f(t) \neq J^{n-\alpha} D^n f(t),$$

then,

$$D^\alpha f(t) \neq D_*^\alpha f(t).$$

**Lemma 1** ([5]). *Let  $n - 1 < \alpha \leq n$ , for any  $n \in \mathbb{N}$  and  $f(t)$  be such that  $D_*^\alpha f(t)$  exists. Then the following properties for the Caputo operator hold ,*

$$\begin{aligned} \lim_{\alpha \rightarrow n} D_*^\alpha f(t) &= f^{(n)}(t), \\ \lim_{\alpha \rightarrow n-1} D_*^\alpha f(t) &= f^{(n-1)}(t) - f^{(n-1)}(0). \end{aligned} \tag{1.8}$$

*Proof.* First,

$$\begin{aligned}
D_*^\alpha f(t) &= \frac{1}{\Gamma(n-\alpha)} \int_0^t \frac{f^{(n)}(\tau)}{(t-\tau)^{\alpha+1-n}} d\tau \\
&= \frac{1}{\Gamma(n-\alpha)} \left( -f^{(n)}(\tau) \frac{(t-\tau)^{n-\alpha}}{n-\alpha} \Big|_{\tau=0}^t + \int_0^t f^{(n+1)}(\tau) \frac{(t-\tau)^{n-\alpha}}{n-\alpha} d\tau \right) \\
&= \frac{1}{\Gamma(n-\alpha+1)} \left( f^{(n)}(0)t^{n-\alpha} + \int_0^t f^{(n+1)}(\tau)(t-\tau)^{n-\alpha} d\tau \right).
\end{aligned} \tag{1.9}$$

We now take the limit as  $\alpha$  approaches  $n$  and  $n-1$ , respectively,

$$\lim_{\alpha \rightarrow n} D_*^\alpha f(t) = f^{(n)}(0) + [f^{(n)}(\tau)]_{\tau=0}^t = f^{(n)}(t), \tag{1.10}$$

and

$$\begin{aligned}
\lim_{\alpha \rightarrow n-1} D_*^\alpha f(t) &= (f^{(n)}(0) + f^{(n)}(\tau)(t-\tau)) \Big|_{\tau=0}^t + \int_0^t f^{(n)}(\tau) d\tau \\
&= f^{(n-1)}(\tau) \Big|_{\tau=0}^t \\
&= f^{(n-1)}(t) - f^{(n-1)}(0).
\end{aligned} \tag{1.11}$$

□

Now, we present some properties of the Caputo derivative.

- **Linearity of Caputo derivative**

**Lemma 2** ([5]). *Let  $n-1 < \alpha \leq n$ , for  $n \in \mathbb{N}$ ,  $c \in \mathbb{R}$  and functions  $f(t)$  and  $g(t)$  be such that  $D_*^\alpha f(t)$  and  $D_*^\alpha g(t)$  exist. Then the Caputo fractional derivative is a linear operator defined as,*

$$D_*^\alpha (cf(t) + g(t)) = cD_*^\alpha f(t) + D_*^\alpha g(t).$$

- **Caputo is non-commutative**

**Lemma 3** ([5]). *Let  $n-1 < \alpha \leq n$ , with  $n, m \in \mathbb{N}$  and function  $f(t)$  be such that  $D_*^\alpha f(t)$  exists.*

*Then,*

$$D_*^\alpha D_*^m f(t) = D_*^{\alpha+m} f(t) \neq D_*^m D_*^\alpha f(t). \tag{1.12}$$

### 1.3 Laplace Transform

The Laplace transform can be used to solve differential equations. It reduces a linear differential equation to an algebraic one which can then be solved by rules of algebra. The transform is written as follows:

$$\mathcal{L}\{f(t)\} = F(s) = \int_0^{\infty} e^{-st} f(t) dt. \quad (1.13)$$

Whereas Laplace transform of the Caputo fractional derivative is given by [4]

$$\mathcal{L}[D_*^\alpha f(t)] = s^\alpha F(s) - \sum_{k=0}^{n-1} f^{(k)}(0) s^{\alpha-k-1}. \quad (1.14)$$

The Laplace transform of the Mittag-Leffler function is given by [4]

$$\mathcal{L}[t^{\beta-1} E_{\alpha,\beta}(\pm \lambda t^\alpha)] = \frac{s^{\alpha-\beta}}{s^\alpha \mp \lambda}. \quad (1.15)$$

#### 1.3.1 Laplace Transform Examples

On Table 1.1 examples of the Laplace transform can be seen. On top of these, other examples can be found in [5].

$f(t)$	$Df$	$D_*^\alpha f$	$\mathcal{L}(f)$	$\mathcal{L}(Df)$	$\mathcal{L}(D_*^\alpha f)$
$c$	$0$	$0$	$\frac{c}{s}$	$0$	$0$
$t$	$1$	$\frac{t^\alpha}{\Gamma(\alpha+1)}$	$\frac{1}{s^2}$	$\frac{1}{s}$	$\frac{1}{s^{\alpha+1}}$
$e^t$	$e^t$	$t^{n-\alpha} E_{1,n-\alpha+1}(t)$	$\frac{1}{s-1}$	$\frac{1}{s-1}$	$\frac{s^{2\alpha-n+1}}{s^\alpha - \alpha}$
$t^n$	$nt^{n-1}$	$nt^{n-\alpha}$	$n!s^{-n-1}$	$n!s^{-n}$	$n!s^{-n-\alpha}$
$n^t$	$n^t \log(n)$	$n^t \log(n)^\alpha e^{t \log(n)}$	$\frac{1}{s - \log(n)}$	$\frac{\log(n)}{s - \log(n)}$	$\frac{\log(n)^\alpha}{s - \log(n)}$

Table 1.1: Laplace transform of various functions, their derivative, and their derivative of fractional order  $\alpha$ .

### 1.3.2 Inverse Laplace Transform

If we have some integrated function  $F(s)$  and wish to retrace back to its pre-integrated form,  $f(s)$ , then we can use the inverse Laplace transform, defined as,

$$f(t) = \mathcal{L}^{-1}\{F(s);t\} := \frac{1}{2\pi i} \int_{c-\infty i}^{c+\infty i} e^{st} F(s) ds, \quad c = \operatorname{Re}(s) > c_0.$$

**Corollary 1.** Let  $n-1 < \alpha \leq n$ ,  $n \in \mathbb{N}$ ,  $0 < \beta = \alpha - (n-1) \leq 1$ , and function  $f(t)$  be such that  $D_*^\alpha f(t)$  exists. Then,

$$D_*^\alpha f(t) = D_*^\beta D_*^{n-1} f(t).$$

*Proof.* Using (1.12), substitute  $\beta$  for  $\alpha$  and  $n-1$  for  $m$ , then

$$D_*^\beta D_*^{n-1} f(t) = D_*^{\beta+n-1} f(t) = D_*^\alpha f(t).$$

□

**Lemma 4.** The Taylor series of a real function  $f(t)$  which is algebraic at a real or complex value  $a$  is the power series,

$$f(t) = f(a) + f'(a)(t-a) + \frac{f''(a)}{2!}(t-a)^2 + \frac{f'''(a)}{3!}(t-a)^3 + \dots,$$

which can be rewritten as,

$$\sum_{n=0}^{\infty} \frac{f^{(n)}(a)}{n!} (t-a)^n,$$

where  $f^{(n)}(a)$  denotes the  $n$ th order derivative of the function  $f$ .

**Proposition 1** ([5]). For  $0 < \alpha \leq 1$ ,

$$D_*^\alpha f(t) = \sum_{k=0}^{\infty} \frac{f^{(k)}(0)}{\Gamma(k-\alpha+1)} t^{k-\alpha}, \quad \text{where } k = 1, 2, 3, \dots \quad (1.16)$$

**Example 1.** For  $f(t) = t^k$  and  $k \in \mathbb{N}$ ,

$$\begin{aligned} D_*^\alpha f(t) &= D_*^\alpha t^k = \sum_{k=0}^{\infty} \frac{f^{(k)}(0)}{\Gamma(k-\alpha+1)} t^{k-\alpha} \\ &= \frac{k!}{\Gamma(k-\alpha+1)} t^{k-\alpha}. \end{aligned} \quad (1.17)$$

**Example 2.** Fix  $\lambda \in \mathbb{R}$ ,

$$f(t) = e^{\lambda t}, \text{ for } t \in \mathbb{R}. \quad (1.18)$$

From Proposition 1,

$$\begin{aligned} D_*^\alpha f(t) &= D_*^\alpha e^{\lambda t} = \sum_{k=0}^{\infty} \frac{f^{(k)}(0)}{k!} D_*^\alpha t^k \\ &= \sum_{k=0}^{\infty} \frac{\lambda^k}{k!} D_*^\alpha t^k \\ &= \sum_{k=0}^{\infty} \frac{\lambda^k}{k!} \frac{\Gamma(k+1)}{\Gamma(k-\alpha+1)} t^{k-\alpha} \\ &= \sum_{k=0}^{\infty} \frac{\lambda^k}{k!} \frac{k!}{\Gamma(k-\alpha+1)} t^{k-\alpha} \\ &= \sum_{k=0}^{\infty} \frac{(\lambda t)^{k-\alpha}}{\Gamma(k-\alpha+1)} t^\alpha \\ &= t^\alpha E_{1,1-\alpha}(\lambda t). \end{aligned} \quad (1.19)$$

Now we turn to solving fractional differential equations.

**Theorem 1** ([2]). Consider the initial value problem

$$\begin{aligned} D_*^\alpha x(t) &= f(t, x(t)), \\ x(0) &= x_0. \end{aligned} \quad (1.20)$$

Let

$$g(v, x_*(v)) = f\left(t - (t^\alpha - v\Gamma(\alpha+1))^{\frac{1}{\alpha}}, x\left(t - (t^\alpha - v\Gamma(\alpha+1))^{\frac{1}{\alpha}}\right)\right). \quad (1.21)$$

Then, a solution of (1.20) is given by

$$x(t) = x_* \left( \frac{t^\alpha}{\Gamma(\alpha + 1)} \right), \quad (1.22)$$

where  $x_*(v)$  is a solution of the integer order differential equation

$$\frac{d(x_*(v))}{dv} = g(v, x_*(v)), \quad (1.23)$$

with initial condition

$$x_*(0) = x_0.$$

*Proof.* Let  $\tau = t - (t^\alpha - v\Gamma(\alpha + 1))^{\frac{1}{\alpha}}$ . Then we can rewrite (1.6)[2]

$$\begin{aligned} x(t) &= x_0 + \int_0^{\frac{t^\alpha}{\Gamma(\alpha+1)}} f(t - (t^\alpha - v\Gamma(\alpha + 1))^{\frac{1}{\alpha}}, x(t - (t^\alpha - v\Gamma(\alpha + 1))^{\frac{1}{\alpha}}) dv \\ &= x_0 + \int_0^{\frac{t^\alpha}{\Gamma(\alpha+1)}} g(v, x_*(v)) dv. \end{aligned} \quad (1.24)$$

Thus, every solution of (1.23) is also a solution of the Volterra integral equation given below and vice versa

$$x_*(v) = x_0 + \int_0^v g(s, x_*(s)) ds, \quad 0 \leq v \leq \frac{a^\alpha}{\Gamma(\alpha + 1)}. \quad (1.25)$$

Since  $0 \leq \frac{t^\alpha}{\Gamma(\alpha+1)} \leq \frac{a^\alpha}{\Gamma(\alpha+1)}$ , the right-hand side of (1.25) is equal to  $x_* \left( \frac{t^\alpha}{\Gamma(\alpha+1)} \right)$ .  $\square$

When using this method of solving a fractional differential equation, the substitution of  $f(\tau)$  is used to turn the problem into the integer-order differential equation (1.23). From then we solve the problem as an ordinary differential equation and end up with (1.24). The integration from 0 to  $\frac{t^\alpha}{\Gamma(\alpha+1)}$  is done because, from (1.22), we know the solution to the original equation is found by this final substitution. Thus, we are able to solve fractional differential equations using this method.

## 1.4 Algorithm

Here, we show the algorithm of the method to solve differential equations used in the Matlab code found in the appendix.

---

**Algorithm 1** Numerical solution of  $D_*^\alpha x(t) = f(t, x(t))$  with  $x(0) = x_0$  for  $0 < t < T$  using Runge-Kutta 4/5<sup>th</sup> order (ode45 solver in MatLab)

---

Input:  $\alpha, T, f(t, x(t)), m, n$

Output:  $x$

**begin**

▷ Divide the interval  $[0, T]$  using  $0 = t_0 < t_1 < \dots < t_n = T$

**for**  $i = 1, 2, \dots, n$

▶ Divide the interval  $[0, \frac{t_i^\alpha}{\Gamma(\alpha + 1)}]$  using  $0 = v_0 < v_1 < \dots < v_m = \frac{t_i^\alpha}{\Gamma(\alpha + 1)}$

▶ Solve the system  $x_*'(v) = f(t_i - (t_i^\alpha - v\Gamma(\alpha + 1))^{\frac{1}{\alpha}}, x_*(v))$  with  $x_*(0) = x_0$  using Runge-Kutta 4/5<sup>th</sup> order

▶ Retain  $x(t_i) = x_*(v_m)$

**end**

▷ Return  $[x_0, x(t_1), x(t_2), \dots, x(t_n)]$

**end**

---

### 1.4.1 Examples of Fractional Differential Equations

**Example 3** ([2]). Consider the fractional order initial value problem given by,

$$\begin{aligned} D^{\frac{1}{2}}x(t) &= t, \\ x(0) &= x_0. \end{aligned} \tag{1.26}$$

For this example,

$$g(v) = 2\sqrt{t}\Gamma\left(\frac{3}{2}\right)v - v^2\Gamma^2\left(\frac{3}{2}\right).$$

*The solution of the corresponding integer order initial value problem is,*

$$x_1(v) = \sqrt{t}\Gamma\left(\frac{3}{2}\right)v^2 - \frac{v^3\Gamma^2\left(\frac{3}{2}\right)}{3} + x_0.$$

*The solution of the given fractional order initial value problem is*

$$x(t) = x_1\left(\frac{t^{\frac{1}{2}}}{\Gamma\left(\frac{3}{2}\right)}\right) = \frac{4t^{\frac{3}{2}}}{3\sqrt{\pi}} + x_0.$$

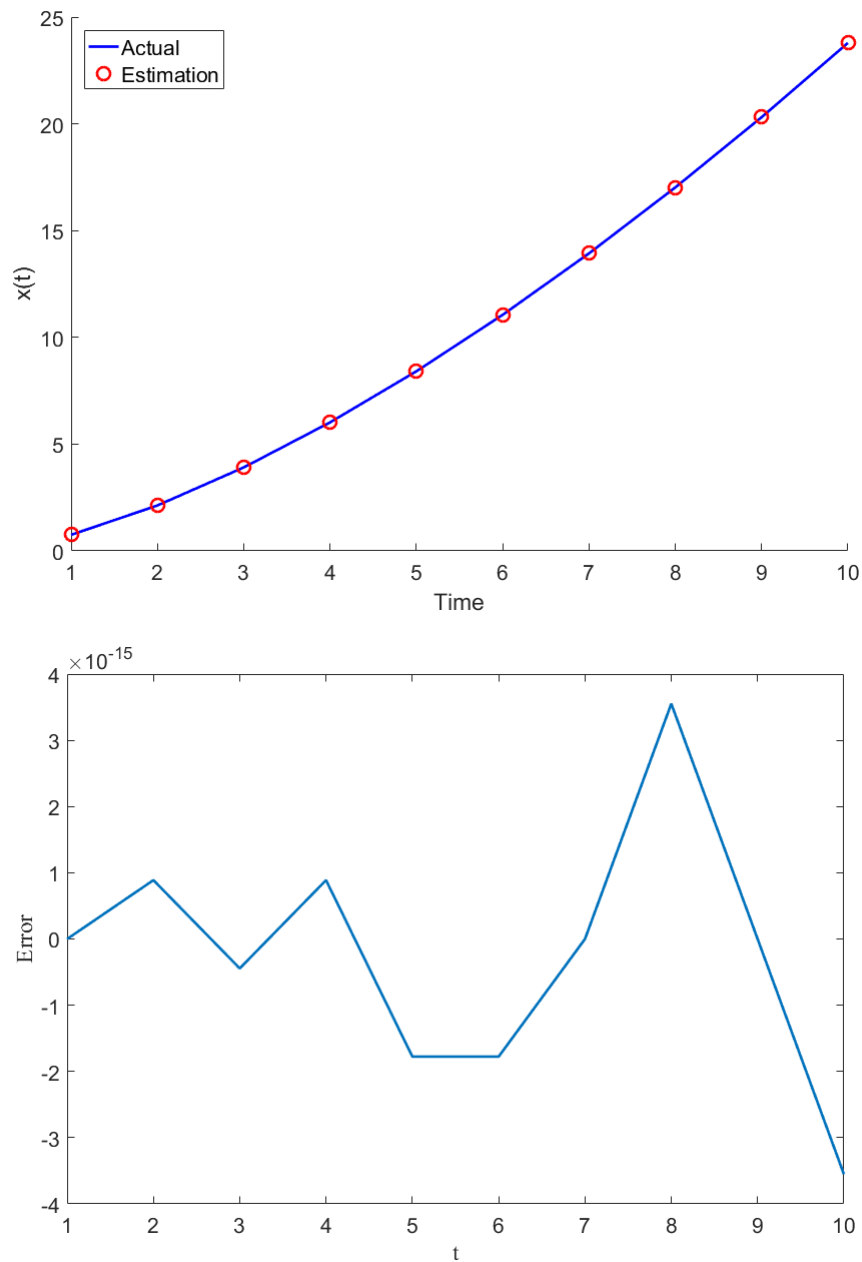


Figure 1.3: Graph of the actual solution compared to the estimate and the error.

From Figure 1.4, it can be seen that the numerical solution overlaps the estimation on the left. This graph shows just how close the numerical solution is to the actual one. Further illustration is seen on the right side graph, where the error is shown to be extremely low. The error is calculated by subtracting the value of the estimated  $x(t)$  by the actual values for each  $t$ .

**Example 4** ([2]). Consider the fractional order initial value problem given by,

$$D^{\frac{1}{2}}x(t) = t + x(t),$$

$$x(0) = x_0.$$

The corresponding differential equation of this fractional initial value problem is

$$\frac{dx_1(v)}{dv} = f_1(v) = x_1(v) + 2\sqrt{t}\Gamma\left(\frac{3}{2}\right)v - v^2\Gamma^2\left(\frac{3}{2}\right),$$

$$x(0) = x_0.$$

Hence, the solutions of this integer order linear initial value problem is

$$x_1(v) = -2\sqrt{t}\Gamma\left(\frac{3}{2}\right)(v+1) + \Gamma^2\left(\frac{3}{2}\right)(v^2 + 2v + 2) + e^v\left(x_0 + 2\sqrt{t}\Gamma\left(\frac{3}{2}\right) - 2\Gamma^2\left(\frac{3}{2}\right)\right),$$

$$x(0) = x_0.$$

Consequently, the solution of the given fractional order initial value problem is

$$x(t) = x_1\left(\frac{t^{\frac{1}{2}}}{\Gamma\left(\frac{3}{2}\right)}\right) = -t + \frac{\pi}{2} + e^{\frac{2\sqrt{t}}{\sqrt{\pi}}}\left(x_0 + \sqrt{t\pi} - \frac{\pi}{2}\right).$$

**Example 5.** An example of nonlinear fractional differential equations describing the process of cooling of a semi-infinite body by radiation is given by [2]

$$D^{\frac{1}{2}}(x(t)) - \alpha(u_0 - x(t))^4 = 0$$

$$x(0) = 0$$

The solution of this problem can be found as

$$x(t) = u_0 - \left( \frac{u_0^3 \sqrt{\pi}}{6\sqrt{t} + \sqrt{\pi}} \right)^{\frac{1}{3}}$$

**Example 6** ([5]). Consider the fractional order initial value problem given by,

$$\begin{aligned} D_*^\alpha x(t) &= \mu x(t), \\ x(0) &= 1, \end{aligned} \tag{1.27}$$

where  $\mu \in \mathbb{R}$ . The solution to (1.27) is given by

$$x(t) = \sum_{k=0}^{\infty} \frac{\mu^k t^{\alpha k}}{\Gamma(\alpha k + 1)} = E_{\alpha,1}(\mu t^\alpha). \tag{1.28}$$

The proof can be found in [5].

### 1.5 Geometrical Interpretation of Fractional Integration

For a long time, integer-order calculus has become the standard when working with most models in most fields. The geometric interpretation has been simple and easy to understand visually. This means that for models of any  $n$ -th order can be covered easily where  $n$  is an integer. Because of this, it only makes sense that a visual understanding of an arbitrary order  $\alpha$  should be found. Now that fields are beginning to use fractional calculus to estimate their models, the need for this visualization has become more necessary. A lot of papers have been published trying to explain or represent fractional calculus visually but most don't hold images representing their words [8]. Because of this, even if you understand the difference in integer and fractional calculus, the difference in geometry is extremely hard to visualize. Igor Podlubny [8] wrote a paper on his approach towards a geometric interpretation for fractional integrals and differentiation. With this approach, he introduces a simple and really geometric interpretation of several fractional-order integration such as the left and right-sided Riemann-Liouville integrals under inhomogeneous and changing time scale. It is suggested that this form of interpretation holds with current views of space and time. With this, a physical approach to Caputo differentiation is also interpreted.

### 1.5.1 Left-sided Riemann-Liouville fractional integral

First, geometric interpretation of left-sided and right-sided Riemann-Liouville fractional integrals [8]. Let us consider the left-sided Riemann-Liouville fractional integral of order  $\alpha$ ,

$${}_0I_t^\alpha f(t) = \frac{1}{\Gamma(\alpha)} \int_0^t f(\tau)(t-\tau)^{\alpha-1} d\tau, \quad (1.29)$$

and rewrite it in the form

$${}_0I_t^\alpha f(t) = \int_0^t f(\tau) dg_t(\tau), \quad (1.30)$$

$$g_t(\tau) = \frac{1}{\Gamma(\alpha)} \{t^\alpha - (t-\tau)^\alpha\}. \quad (1.31)$$

If we take  $t_1 = kt$  and  $\tau_1 = k\tau$ , then

$$g_{t_1}(\tau_1) = g_{kt}(k\tau) = k^\alpha g_t(\tau). \quad (1.32)$$

Let us take the axes  $\tau$ ,  $g$ , and  $f$  from Figure 1.4. In the plane  $(\tau, g)$  we plot the function  $g_t(\tau)$  for  $0 \leq \tau \leq t$  and where  $t$  is fixed. Podlubny describes the curve obtained as a "fence" of varying height  $f(\tau)$ , so the top edge of the "fence" is a three-dimensional line  $(\tau, g_t(\tau), f(\tau))$ ,  $0 \leq \tau \leq t$ . In this, the fence can be projected onto the two surfaces as seen on Figure 1.4 [8]:

- the area of the projection of the fence on the plane  $(\tau, f)$  corresponds to the value of the integral

$${}_0I_t^1(t) = \int_0^t f(\tau) d\tau; \quad (1.33)$$

- the area of the projection of the fence on the other plane  $(g, f)$  corresponds to the value of the integral (1.30) or (1.29).

It should also be said that the fence throws two shadows on the two mentioned walls as seen on Figure 1.4. The former is the recognized integer-order integral and its standard geometric

representation. Whereas, the latter shadow is representing the geometric representation of the fractional integral (1.29) [8].

Note that for  $g_t(\tau) = \tau$ , both shadows are equal in area. This shows that classical definite integration is a particular case of the left-sided Riemann-Liouville fractional integration even from the geometric point of view.

This raises the question, "What if  $t$  wasn't fixed?" If  $t$  were to increase, then the shadows change with the fence. The length, the height, or in general the whole shape would possibly change and so would its shadows.

### 1.5.2 Right-sided Riemann-Liouville fractional integral

Let us consider the right-sided Riemann-Liouville fractional integral [8],

$${}_t I_0^\alpha f(t) = \frac{1}{\Gamma(\alpha)} \int_t^b f(\tau)(\tau - t)^{\alpha-1} d\tau, \quad (1.34)$$

and rewrite it in the form

$${}_t I_0^\alpha f(t) = \int_t^b f(\tau) dh_t(\tau), \quad (1.35)$$

$$h_t(\tau) = \frac{1}{\Gamma(\alpha + 1)} \{t^\alpha + (\tau - t)^\alpha\}. \quad (1.36)$$

Like before, we can now provide a geometric interpretation similar to the one used for the left-sided Riemann-Liouville fractional integral. In this case, there is no fixed point in the fence basis. The end, corresponding to  $\tau = b$ , moves along the line  $\tau = b$  in the plane  $(\tau, g)$  when the fence is changing shape. This type of movement is observed in Figure 1.7. Because  $t$  is fixed in the left-sided integral, the left end which corresponds to  $\tau = 0$  is fixed and does not move. Besides this, all other parts of the geometric interpretation remains the same. The fence's shape is changed as  $t$  changes from 0 to  $b$  and the shadows also change accordingly on the two walls  $(g, f)$  and  $(\tau, f)$  which corresponds to the right-sided integral (1.34) and the classical integral with the moving lower limit [8]:

$$I_b^1(t) = \int_t^b f(\tau) d\tau. \quad (1.37)$$

Just how  $g_t(\tau) = \tau$  shows both shadows being equal on the left-sided integral's visual representation, it can be shown the same when  $h_t(\tau) = \tau$  for the right-sided integral.

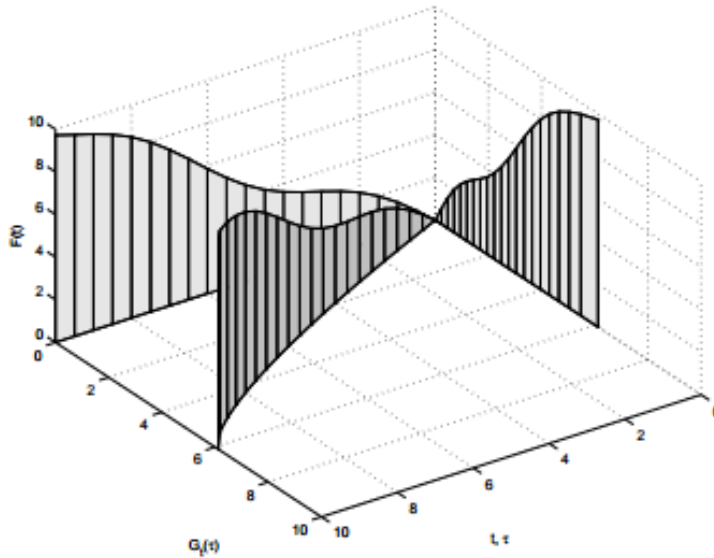


Figure 1.4: The fence and its shadows:  $I_t^1 f(t)$  and  $I_t^\alpha f(t)$ , for  $\alpha = \frac{3}{4}$ ,  $f(t) = t + \frac{\sin(t)}{2}$  [8].

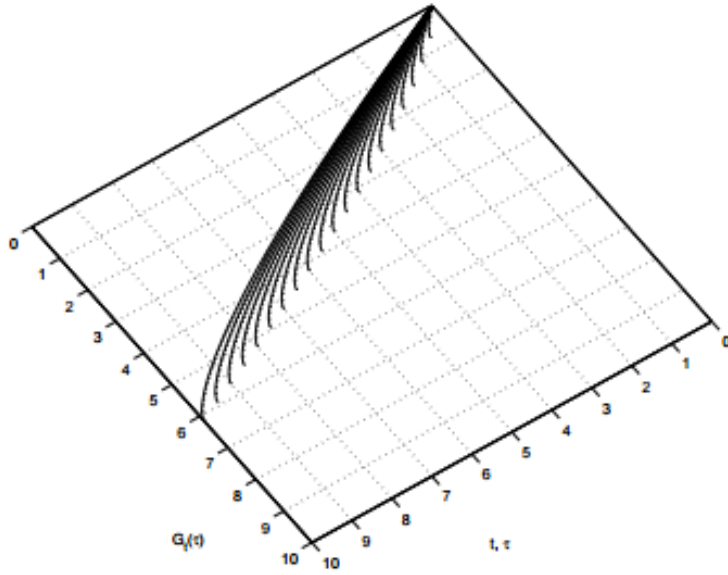


Figure 1.5: The process of change of the fence's basis shape for  $I_t^\alpha f(t)$ ,  $\alpha = \frac{3}{4}$  [8].

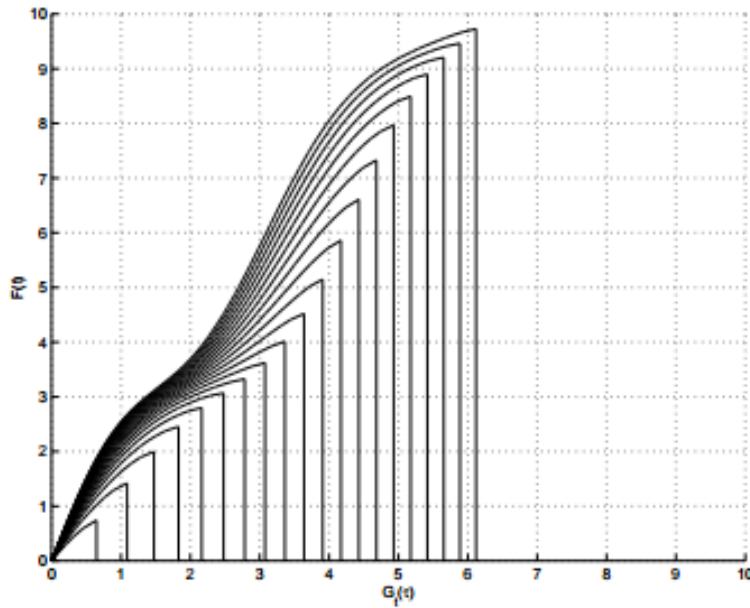


Figure 1.6: Snapshots of the changing shadow of a changing fence for  $I_t^\alpha f(t)$ ,  $\alpha = \frac{3}{4}$ ,  $f(t) = t + \frac{\sin(t)}{2}$ , with time interval  $\Delta t = \frac{1}{2}$  between the snapshots [8].

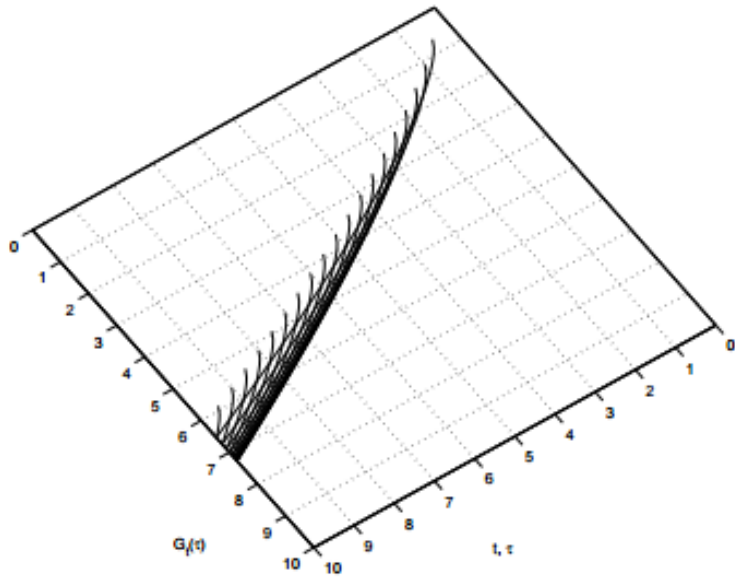


Figure 1.7: The process of change of the fence's basis shape for  ${}_t I_{10}^\alpha f(t)$ ,  $\alpha = \frac{3}{4}$ [8].

## CHAPTER II

### EPIDEMIOLOGICAL MODELS

#### 2.1 SEIR Model

Mathematical models can help understand how the disease spreads in a population. Several models exist and each have their own type of disease they work best with. Within these models the two most used are the SIR and the SEIR. The model we will be using is the SEIR model. The name SEIR serves as an acronym for its four categories it comprises: susceptible, exposed, infectious, and recovered compartments [6]. Figure 2.1 depicts the flow of individuals from one compartment to the next with the recruitment of new susceptible individuals through birth at rate  $\mu$ . This compartment, like all other compartments, have a natural death rate  $\mu$ . The individuals that successfully contact the disease become exposed are then moved to compartment E at the transmission rate of  $\beta N$ , where  $N$  is the total population size. After a latent period with average length  $\frac{1}{\delta}$ , the exposed then become infected/infective, thus moving to compartment I at rate  $\delta$ . Lastly, from compartment I, those who recover from the disease get moved to compartment R at rate  $\sigma$ . So then why the SEIR model over SIR? The most notable difference is the missing 'E' in SIR. The reason why this model does not have an exposed compartment is because the diseases this model works best with are those which show symptoms instantly, whereas some disease take time to surface. Because the nature of the disease this paper will look at, it is better to consider the latent period and use SEIR.

The movement from one compartment to another can be expressed through a system of fractional differential equations, with  $0 < \alpha < 1$ ,

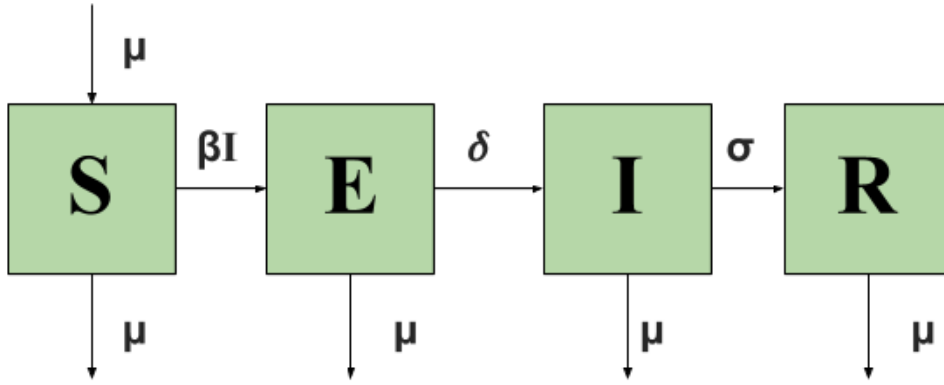


Figure 2.1: This model displays the compartmental flow of the SEIR model.

$$\begin{aligned}
 D_*^\alpha S &= \mu - \beta SI - \mu S \\
 D_*^\alpha E &= \beta SI - (\mu + \delta)E \\
 D_*^\alpha I &= \delta E - (\mu + \sigma)I \\
 D_*^\alpha R &= \sigma I - \mu R
 \end{aligned} \tag{2.1}$$

**Note.** When considering the dimension of parameters  $\mu$ ,  $\delta$ ,  $\sigma$ , and  $\beta$  it has been defined as  $\frac{1}{time}$  when working with systems of integer-order differential equations. However, as we are working with a fractional-order system, the dimension changes. From an integer-order system we have

$$\frac{dI}{dt} = \delta E - (\mu + \sigma)I, \tag{2.2}$$

where the dimensions of the parameters are  $\frac{1}{time}$ . When the system is changed into a fractional-order system

$$D_*^\alpha I = \delta_* E - (\mu_* + \sigma_*)I, \tag{2.3}$$

the parameters are actually the integer-order system's parameters to the power  $\alpha$  where  $n - 1 < \alpha \leq n$ . So then

$$[\mu_*] = [\delta_*] = [\sigma_*] = [\beta_*] = \frac{1}{time^\alpha} \tag{2.4}$$

In (2.1) S, E, I, and R are the proportion of susceptible, exposed, infectious, and recovered. Then

$S + E + I + R = 1$ . Thus, the last equation is redundant.

We state several basic definitions and theorems on the stability of fractional order linear systems [4].

Let  $A \in \mathbb{R}$ ,

$$\begin{aligned} D_*^\alpha x(t) &= Ax(t), \\ x(0) &= x_0. \end{aligned} \tag{2.5}$$

**Definition 1.** [4] We say that (2.5) is stable if for all  $\varepsilon > 0$ ,  $\delta > 0$  exists such that  $\|x_0\| < \delta$ ; then  $\|x(t)\| < \varepsilon$ , for all  $t \geq 0$ ; linear system (2.5) is asymptotically stable if  $\lim_{t \rightarrow \infty} x(t) = 0$ .

**Theorem 2** ([4]). System (2.5) is asymptotically stable if and only if  $|\arg(\lambda_i)| > \frac{\alpha\pi}{2}$  is satisfied for all eigenvalues of matrix  $A$ . Moreover, the system is also stable if and only if  $|\arg(\lambda_i)| > \frac{\alpha\pi}{2}$  is satisfied for all eigenvalues of the matrix  $A$  and the eigenvalues satisfying  $|\arg(\lambda_i)| > \frac{\alpha\pi}{2}$  have geometric multiplicity equal to one.

Consider the following system of fractional order,

$$\begin{aligned} D_*^\alpha x(t) &= f(x), \\ x(0) &= x_0. \end{aligned} \tag{2.6}$$

**Definition 2.** [4]  $E$  is an equilibrium point for (2.6), if and only if  $f(E) = 0$ .

**Remark 2.** [4] When  $\alpha \in (0, 1)$ , the fractional system  $D_*^\alpha x(t) = f(x)$  has the same equilibrium points as the system  $x'(t) = f(x)$ .

**Definition 3.** The equilibrium point  $E$  of (2.6) is said to be stable if for all  $\varepsilon > 0$ ,  $\delta > 0$ , exists such that if  $\|x_0 - E\| < \delta$ , then  $\|x(t) - E\| < \varepsilon$ ,  $t \geq 0$ ; the equilibrium point  $E$  of (2.6) is said to be asymptotically stable if  $\lim_{t \rightarrow \infty} x(t) = E$ .

**Theorem 3.** [4] The equilibrium points of (2.6) are locally asymptotically stable if all eigenvalues  $\lambda_i$  of a Jacobian matrix  $J$ , calculated in the equilibrium points, satisfy  $|\arg(\lambda_i)| > \frac{\alpha\pi}{2}$ .

**Lemma 5.** *The closed region  $M = \{(S, E, I) \in \mathbb{R}_+^3 : 0 \leq S + E + I \leq 1\}$  is a positive invariant set.*

*Proof.* If  $E(0) = I(0) = 0$  and  $1 \geq S(0) = S_0 \geq 0$ , Then on the S-axis using (1.27) and Theorem 4.2 in [3],

$$S(t) = t^\alpha E_{\alpha, \alpha+1}(-\mu t^\alpha)(\mu) + E_{\alpha, 1}(-\mu t^\alpha)S(0) \geq 0$$

since  $\mu > 0, t \geq 0$ .

If  $S(0), I(0) = 0$  and  $E(0) = E_0 \geq 0$ . On the E-axis,

$$E(t) = E_{\alpha, 1}(-(\mu + \delta)t^\alpha)E(0) \geq 0$$

If  $S(0), E(0) = 0$  and  $I(0) = I_0 \geq 0$ . On the I-axis,

$$I(t) = E_{\alpha, 1}(-(\mu + \sigma)t^\alpha)I(0) \geq 0$$

Thus, all axes are positive invariant, for  $S(0), E(0), I(0) \geq 0$ .

If it escapes from E-I plane, then  $S(t_e) = 0$  and  $E(t_e), I(t_e) > 0$  for some  $t_e > 0$  such that for all  $t > t_e$  we have  $S(t) \leq S(t_e)$ . Then  $D_*^\alpha S|_{t=t_e} = \mu > 0$ .

From Lemma 9 in [4] and (1.6) we have

$$S(t) = S(t_e) + \frac{1}{\Gamma(\alpha)} (D_*^\alpha S(\tau)(t - t_e)^\alpha \text{ for } t_e \leq \tau < t$$

for some  $t_e \leq \tau < t$ , then  $S(t) > S(t_e)$  contradicting the original statement. The same could be said with  $D_*^\alpha E|_{t=t_e} = \beta S(t_e)I(t_e) > 0$  and  $D_*^\alpha I|_{t=t_e} = \alpha E(t_e) > 0$ .

To show  $S + E + I \leq 1$ , if  $S(0) + E(0) + I(0) \leq 1$ ,

$$\begin{aligned} D_*^\alpha (S + E + I) &= \mu - \mu(S + E + I) - \sigma I \\ &\leq \mu - \mu(S + E + I) \end{aligned} \tag{2.7}$$

Using the Laplace transform property in (6)-(7) from [4],

$$\begin{aligned} S(t) + E(t) + I(t) &\leq t^\alpha E_{\alpha, \alpha+1}(-\mu t^\alpha) \mu + E_{\alpha, 1}(-\mu t^\alpha) (S(0) + E(0) + I(0)) \\ &\leq t^\alpha E_{\alpha, \alpha+1}(-\mu t^\alpha) \mu + E_{\alpha, 1}(-\mu t^\alpha) = 1 \end{aligned} \quad (2.8)$$

□

## 2.2 Stability Analysis of a Disease-Free Equilibrium

For the local stability of a disease-free equilibrium, we must evaluate the Jacobian matrix at

$$E_{DF} = (1, 0, 0)$$

$$J(E_{DF}) = \begin{bmatrix} -\mu & 0 & -\beta \\ 0 & -(\mu + \delta) & \beta \\ 0 & \delta & -(\mu + \sigma) \end{bmatrix}$$

The disease free equilibrium  $E_{DF}$  is locally asymptotically stable if  $|\arg(\lambda)| > \frac{\alpha\pi}{2}$ , for  $i = 1, 2, 3$ .

$$|J(E_{DF}) - \lambda I| = \det \begin{bmatrix} -\mu - \lambda & 0 & -\beta \\ 0 & -(\mu + \delta) - \lambda & \beta \\ 0 & \delta & -(\mu + \sigma) - \lambda \end{bmatrix} = 0$$

The eigenvalues of the matrix are,

$$\begin{aligned} \lambda_1 &= -\mu, \\ \lambda_2 &= \frac{-(\delta + 2\mu + \sigma) - \sqrt{\Delta}}{2}, \\ \lambda_3 &= \frac{-(\delta + 2\mu + \sigma) + \sqrt{\Delta}}{2}, \end{aligned}$$

where  $\Delta = \delta^2 + 4\delta\beta - 2\delta\sigma + \sigma^2$ . From this it is clear that  $\lambda_1$  is negative and because  $\delta > 0$ ,  $\lambda_2$  and  $\lambda_3$  are real-valued, since

$$\Delta = \delta^2 + 4\delta\beta - 2\delta\sigma + \sigma^2 = (\delta - \sigma)^2 + 4\delta\beta > 0.$$

Hence  $\lambda_2 < 0$  and it can be inferred that,

$$\begin{aligned} \lambda_3 &= \frac{-(\delta + 2\mu + \sigma) + \sqrt{\Delta}}{2} \\ &< \frac{-(\delta + 2\mu + \sigma) + \sqrt{(\delta + 2\mu + \sigma)^2}}{2} \\ &= \frac{-(\delta + 2\mu + \sigma) + \delta + 2\mu + \sigma}{2} = 0. \end{aligned}$$

Since  $\lambda_3 < 0$ , we can see all eigenvalues of the Jacobian matrix  $E_{DF}$  are negative, and so  $|\operatorname{Re}(\lambda_i)| < 0$ ,  $i = 1, 2, 3$ . This implies that  $|\arg(\lambda_i)| > \alpha \frac{\pi}{2}$  for all  $i$  and any  $0 < \alpha \leq 1$ .

## CHAPTER III

### SIMULATIONS AND ESTIMATION

The purpose of this chapter is to display the effect  $\alpha$  and  $\beta$  both have on the model. As mentioned before fractional calculus adds a memory effect onto the model which helps fit specific diseases and the speed at which a person moved from one compartment to another. Figures 3.2-3.6 show this effect. First, it is important to show how the different models look when being graphed. Figure 3.1 shows the SIR and SEIR models being graphed in the same order.

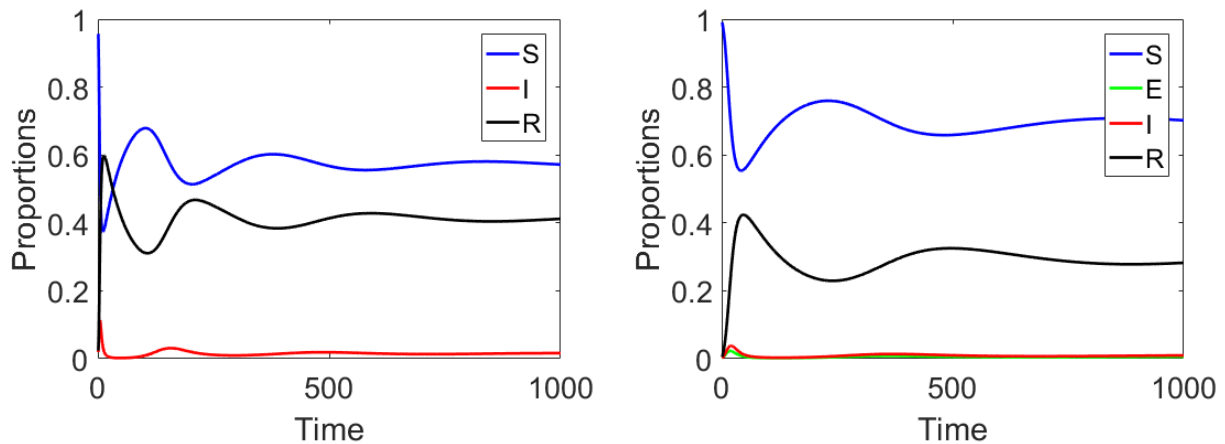


Figure 3.1: Graph of the SIR model and SEIR model using  $\alpha = \frac{1}{2}$  and  $\beta = 40$ .

The disease fades out in both SIR and SEIR, since the values of the parameters entail that the disease free equilibrium is stable. Because of this, the exposed follow the trend over time. Again, because of the diseases in mind when performing this research, the SEIR model was used.

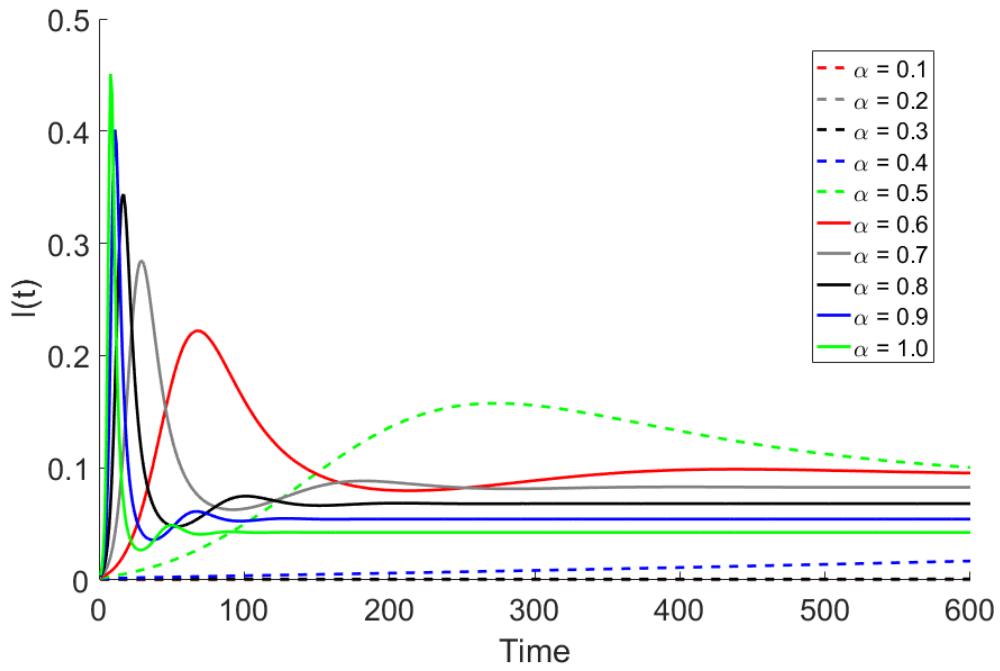


Figure 3.2: Numerical solution of  $I$  when  $\beta^\alpha = 5$  for different values of  $\alpha$ .

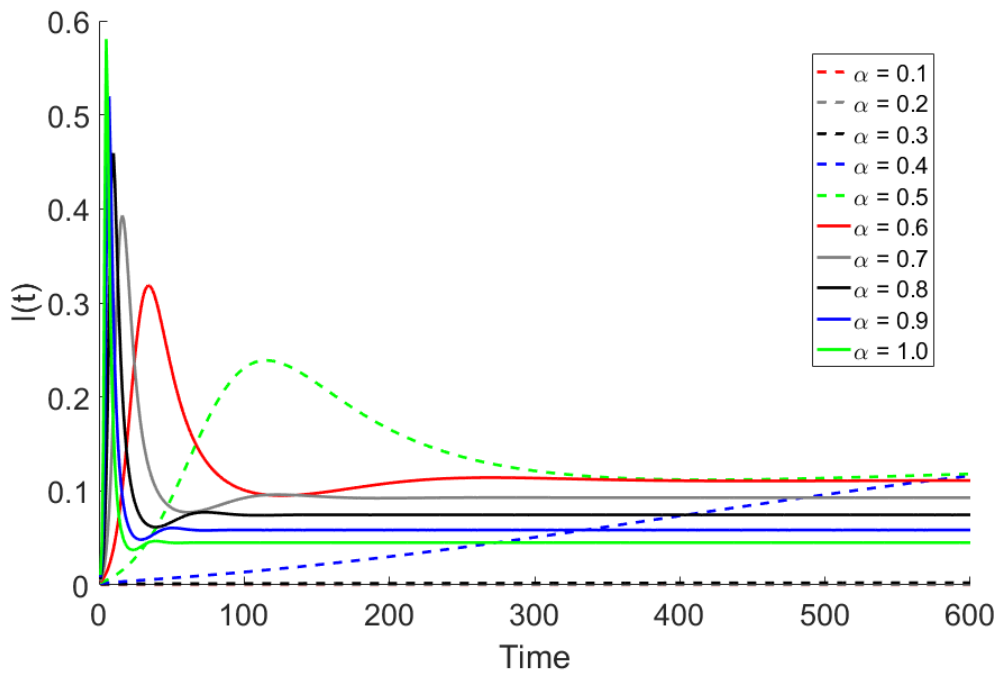


Figure 3.3: Numerical solution of  $I$  when  $\beta^\alpha = 10$  for different values of  $\alpha$ .

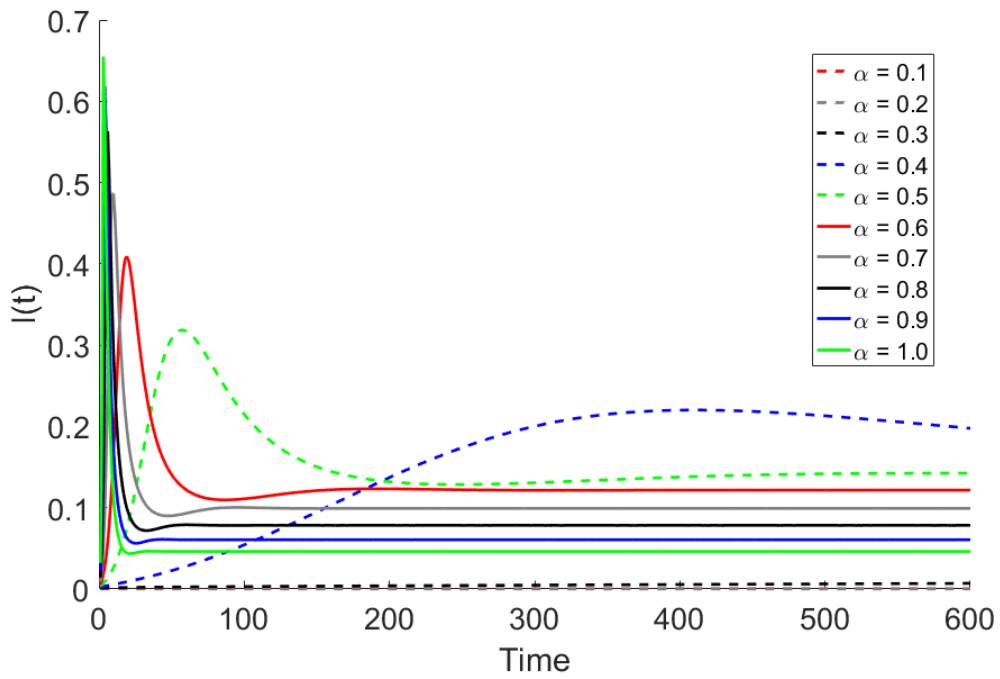


Figure 3.4: Numerical solution of  $I$  when  $\beta^\alpha = 20$  for different values of  $\alpha$ .

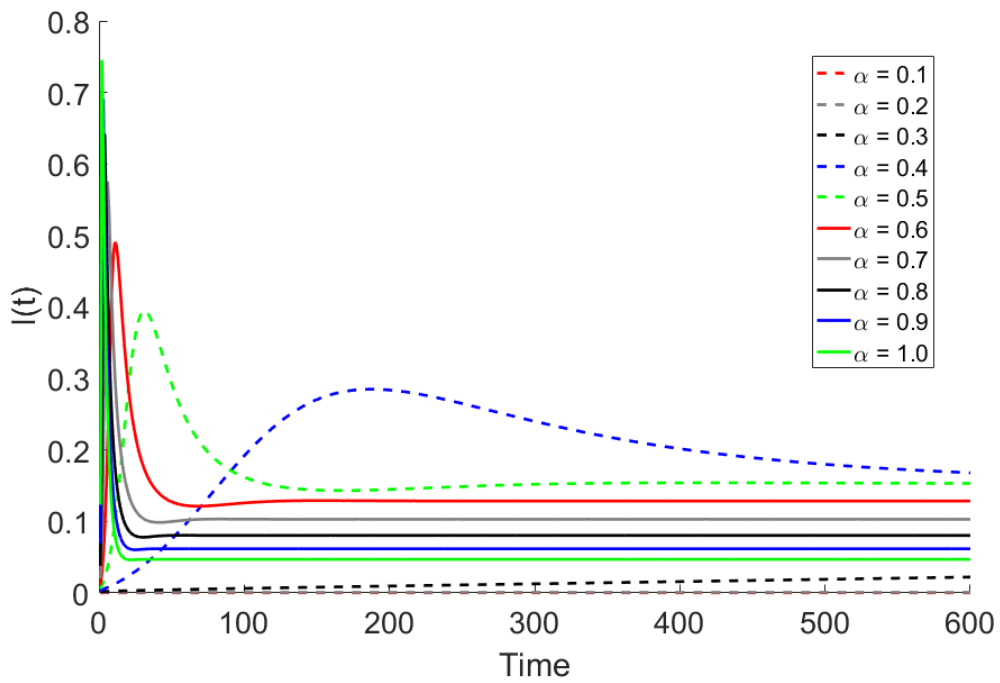


Figure 3.5: Numerical solution of  $I$  when  $\beta^\alpha = 40$  for different values of  $\alpha$ .

In this paper, different values of  $\alpha$  were compared using increasing values of  $\beta^\alpha$ . It can be seen that as  $\alpha$  increases, a higher peak of infection is reached at an increased rate. When simulating under a higher  $\beta^\alpha$ , the rate of infection for different values of  $\alpha$  are closer to one another and the equilibrium and peak are reached at earlier times. The time difference in reaching equilibrium displays the memory effect in these models. Depending on the disease one chooses to work with, the time it moves from one compartment to another could vary. Different values of  $\beta^\alpha$  and  $\alpha$  could better fit those diseases. Using integer-order differential equations to estimate these models only follows exponential distributed curves which may not fit every disease. Using fractional-ordered equations allow this flexibility to better fit different diseases as shown through heavy tail distribution. This type of effect has become increasingly useful in several fields. These simulations are made to show the relationship between  $\alpha$  and  $\beta^\alpha$ , but it is important to test a value of  $\beta^\alpha$  where  $R_0 < 1$  to numerically support the claims in our disease free equilibrium calculations.

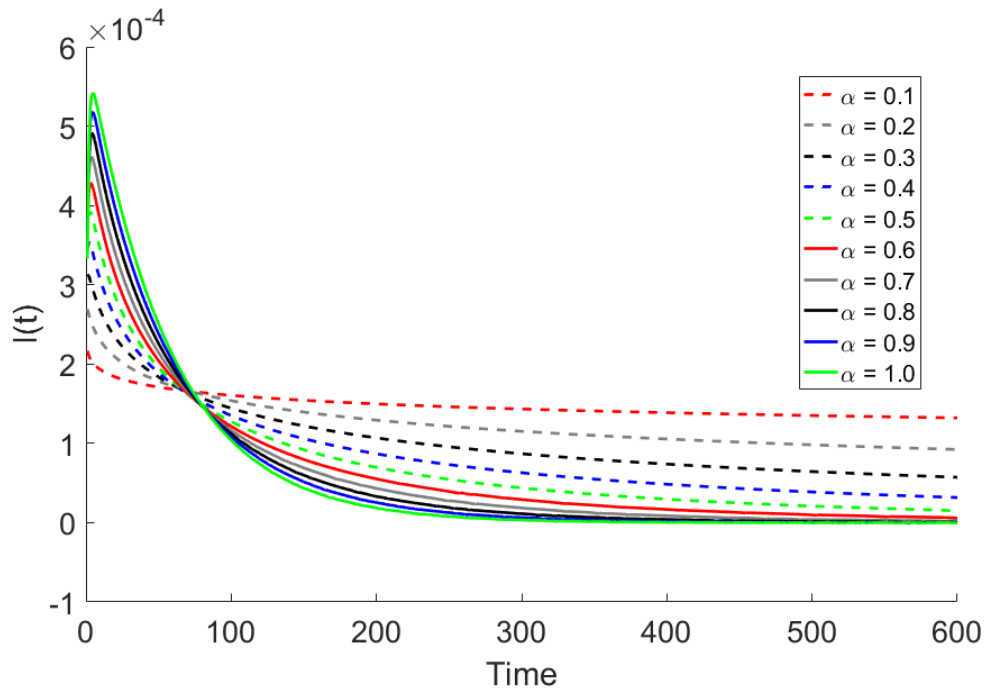


Figure 3.6: Numerical solution of  $I$  when  $\beta^\alpha = 0.5$  and  $R_0 < 1$  for different values of  $\alpha$ .

Through simple algebra, we get  $S = \frac{(\mu+\sigma)(\mu+\delta)}{\beta\delta} = \frac{1}{R_0}$ . We use this to find a suitable  $\beta < R_0$  to test. In this case, we chose  $\beta^\alpha = 0.5$ .

### 3.1 Estimation: Nonlinear Least Squares Method

The nonlinear least squares problem takes the form of

$$\underset{x}{\text{minimize}} f(x) = \sum_{j=1}^m r_j(x)^2. \quad (3.1)$$

It is called least squares because we are minimizing the sum of squares for these functions [1]. Given a set of data  $d(t_j, y_j)$  and a model function  $\phi(x; t_j)$  the difference of the functions is obtained with  $r_j(x) = \phi(x; t_j) - y_j$ , where  $y_j$  is the y component of the data at point  $t_j$ . The objective function of least squares problems is therefore

$$f(x) = \frac{1}{2} \sum_{j=1}^m r_j^2(x). \quad (3.2)$$

Through minimizing the function  $f$ , parameters that match the model of the observed data best can be found. Each  $r_j$  is called a residual. They are smooth functions from  $\mathbb{R}^n$  to  $\mathbb{R}$ . Now (3.2) can be rewritten using the residual vector  $f(x) = \frac{1}{2} \|r(x)\|_2^2$  [1].

In the appendix, the code for this method can be seen in ESS. The function is called with a vector of two parameters,  $\alpha$  and  $\beta$  representing  $\alpha$  and  $\beta$  respectively. The model is then simulated with the estimated values of  $\alpha$  and  $\beta$  and compared to the actual simulation. Then to fit the sum of squares "fminsearch" is ran with the sum of resid squared which is the same as the residue vectors  $r_j(x)$  from (3.1) and (3.2).

### 3.2 Akaike Information Criterion

On 1973, Hirotugu Akaike published a paper discussing a new information criterion. It eventually became known as the Akaike information criterion (AIC). This was introduced with the intention of estimating information lost when simulating data through a model. The AIC can be calculated by

$$AIC = 2k - 2\ln(M),$$

where  $M$  is the maximum value of the likelihood function and  $k$  is the number of estimated parameters in the model. A few years later, another publication was released in which the AICc was discussed. This was like AIC with a correction for finite sample sizes. Although the formula for the AICc depends on the type of model being used, under the assumption that the model is univariate, linear, and has normally-distributed residuals, the formula is written

$$AICc = AIC + \frac{2k(k+1)}{n-k-1},$$

where  $n$  denotes the sample size. Eventually, the Bayesian information criterion (BIC) was discovered. The BIC is defined as

$$BIC = \ln(n)k - 2 \ln(M).$$

Similar to the AIC, the BIC is used to measure the efficiency of the parameterized model to predict data. This criterion, however, penalizes the model more than the AIC. So what this means is, although the model could possibly increase the likelihood by adding parameters during fitting, it may also result in overfitting. This is considered to be an error when the model becomes overly complex and the predictive performance reacts harshly to minor fluctuations in the data.

### 3.3 Results

As mentioned in chapter 2, the natural immunity variable  $\gamma$  in the SEIR model was removed for simplicity. Over the lapse of this research it was hard to find raw data for the disease we could work with prior to the date in which the vaccination was made and distributed. Initially the disease in mind was measles; but because the vaccine was created in 1963, finding data from an epidemic much earlier than that proved to be difficult. Although other diseases were also searched for, none of them had data prior to vaccination. Unfortunately because of this situation, our results are based on simulated data. Graphs with different  $\alpha$  and  $\beta$  values were tested and displayed in Figures 3.1 through 3.6. However, this was just showing the simulation side of the code used. Those figures were made to show the different effects changing those two variables had to models, but it is also important to have code to estimate those values off of a model of fractional differential equation.

$\alpha$	$\beta$	$\alpha$ Estimated	$\beta$ Estimated	AICc	BICc	Percent Error
.1	.5	.1	.5	$-\infty$	$-\infty$	0
.1	30	.1	30	$-\infty$	$-\infty$	0
.1	40	.1	40	$-\infty$	$-\infty$	0
.5	20	.5	20	$-\infty$	$-\infty$	0
.5	30	.5	30	$-\infty$	$-\infty$	0
.5	40	.5	40	$-\infty$	$-\infty$	0
1	20	1	20	$-\infty$	$-\infty$	0
1	30	1	30	$-\infty$	$-\infty$	0
1	40	1	40	$-\infty$	$-\infty$	0

Table 3.1: Actual values, estimated values, and the error between them

On Table 4.1, one can see the different  $\alpha$  and  $\beta$  values used to simulate a model, as well as work backwards and find them off of the model created using those values. For this reason, the AICc, BICc, Error, and final values of the estimated  $\alpha$  and  $\beta$  are also displayed on Table 4.1 to show the accuracy the code used has.

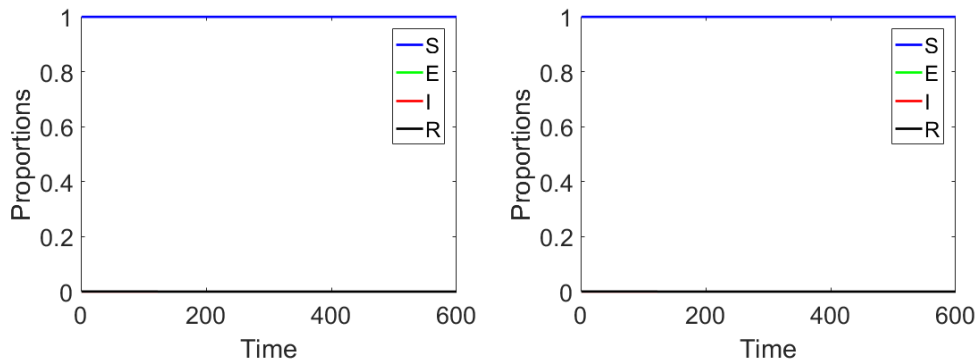


Figure 3.7: Side by side comparison of the model when  $\alpha = .1$  and  $\beta^\alpha = .5$ .

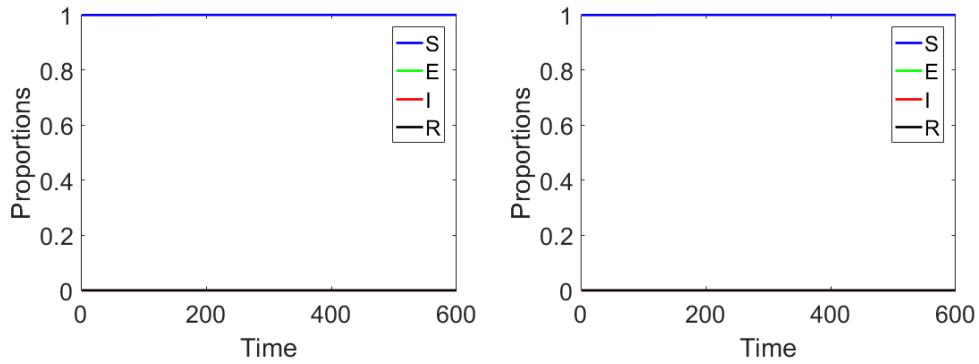


Figure 3.8: Side by side comparison of the model when  $\alpha = .1$  and  $\beta^\alpha = 30$ .

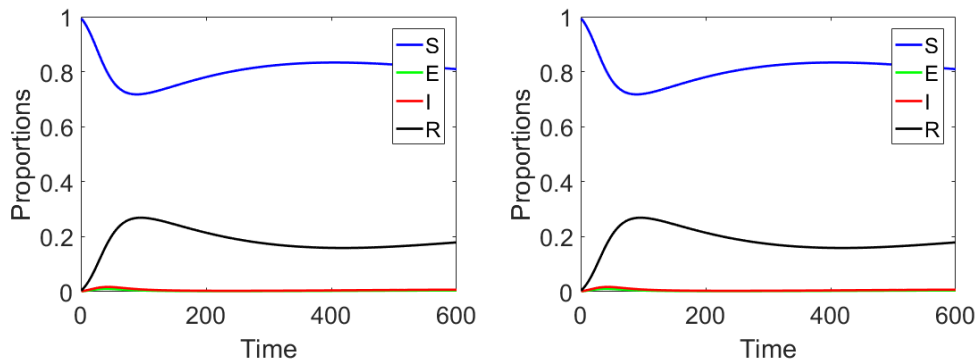


Figure 3.9: Side by side comparison of the model when  $\alpha = .5$  and  $\beta^\alpha = 30$ .

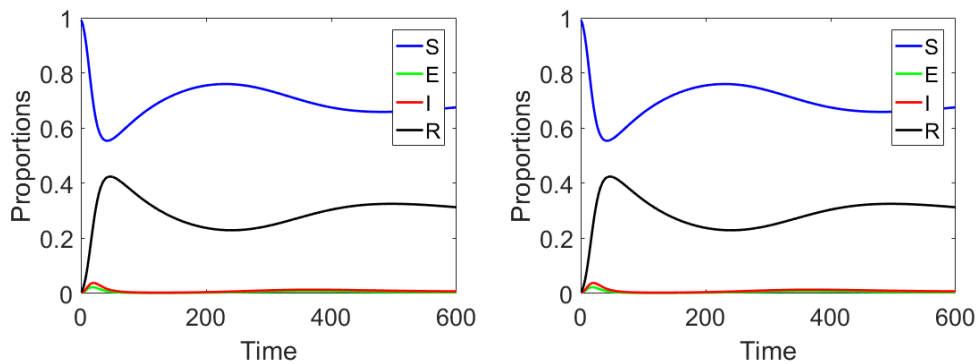


Figure 3.10: Side by side comparison of the model when  $\alpha = .5$  and  $\beta^\alpha = 40$ .

As shown on Table 4.1, there was error of 0 for all these examples. This means the code used was most accurate when estimating the  $\alpha$  and  $\beta^\alpha$  when solving a system of fractional differential

equations in an SEIR model. The estimated values are all the same to the actual ones being solved for as can be seen from Figures 3.7 - 3.10.

### 3.4 Data

The MatLab code used to calculate these estimations and produce the graphs shown in this paper can be found in the appendix. This section will go over what each code contributes towards the research and what it all does file by file.

Taking a look at the first code, `mainFrac2`, the first two lines are just to clear any cache data on the system. Under the note of "Simulation", time  $T$  is adjusted to the type of figure needed. For the estimations, I used  $T = 600$  to show a the model, Figures 4.2 through 4.5 used  $T = 150$  to show when the infected reach equilibrium, but for Figure 4.6 a much higher  $T$  was needed to show the delayed reach in equilibrium by other values of  $\alpha$ . The variable "y<sub>not</sub>" is used for proportions of the model. The four values are meant for the susceptible, exposed, infected, and recovered compartments respectively. Variables "a" and "b" represent the  $\alpha$  and  $\beta$  values used in the model. The model can be found in the file `odeFrac2`, but is called and solved for in `solodeFrac`. The matrix output by `solodeFrac` is then registered under matrix "x". Variable "z" is only used to copy "x" and removed the collective vector which is not needed to graph. It is then graphed through "createfigure1" with the preferred settings. This has been all for the simulation portion of the code. These solutions are the actual solutions compared to after running the estimation part of this code.

This portion of the code is what we tested for accuracy in Section 5.1. In all these files, variables "T", "actual", and "y<sub>not</sub>" are global. This means they are shared through all the files. The former and latter variable were already introduced as time and the proportions of the model, where "actual" holds the same values as "z", or the four compartment mentioned from "x". Earlier  $\alpha$  and  $\beta$  were introduced for simulations, to find those two values through estimation, "a0" and "beta0" are introduced as starting points for the program to work around. When calling a function from another code, like ESS or `solodeFrac`, parameters and options are needed for the code to have some guidance in how one wants the program to run and return values. For this, "options" is created with the specific values we want to work around. The first two options are the tolerance in the solutions.

The lower the tolerance, the more precise the code tries to be. Naturally, a low quantity is entered so we get as precise as possible. Note that all options that begin with single quotes refer to the name of the option we are setting up. The next options are regarding the maximum number of iterations we want the program to run for and also the maximum number of evaluations done by the program. For these two, the higher the number assigned the better, but just like having a lower tolerance, it takes a lot out of your computer to run this. Initially the code ran this with a maximum iteration of 3000, meaning it would run the optimization at most 3000 times to ensure the smallest error and highest precision possible. After testing different estimations for varied pairs of  $\alpha$  and  $\beta$ , a steep diminishing return was found due to the code already being optimal around 100 iterations. So instead of running one estimation for 4 to 6 hours and still be in iteration 1000 with an error value low enough to approximate zero, it was lowered down to 120 to keep low enough values for error as shown on Table 5.1 and save time. Once setting up the options for the function, we call the function "ESS" we use the values introduced to use the sum of squared errors of prediction and find the values of interest. The output then gives "phat" the values of the discovered  $\alpha$  and  $\beta$  as well as the error found in the function. As introduced in Section 4.2, the formulas for the Akaike information criterion and the Bayesian information criterion are used next. This part gives the accuracy of your results and information lost. Lastly, similar to the simulation part of the code, the estimated model is given to matrix "y" and graphed with the preferences wanted and then the simulated and estimated models are compared with createfigureError.

## CHAPTER IV

### CONCLUSION AND FUTURE WORK

From the difference in distribution for epidemic models using fractional or integer-order differential equations, it can be seen from Figures 3.2 - 3.6 how fractional calculus is worth taking into consideration. The memory effect the fractional-order differentiation can be used to better fit specific diseases and their latent period in jumping from one compartment to the next. Because some diseases may peak faster than others, the option to change order of differentiation for better fitting. Unfortunately, for this paper raw data prior to vaccination was not found. So having to simulate the data and then attempting to estimate the values for  $\alpha$  and  $\beta$  proved the code to be accurate in Table 3.1. The next step would be to contact authors who have used their private data and test the code. Another possibility, is to further update the code to be able to work with different models and eventually with inclusion of the natural immunity variable  $\gamma$ .

## APPENDIX A

## APPENDIX A

### MATLAB CODE

To give the results credibility, as well as share the code to anyone interested in continuing this research on their own, the data is included for anyone to use.

#### **mainFrac.m**

```
clear all
```

```
clc
```

```
% Simulation
```

```
tic
```

```
T=600;
```

```
ynot = [1 -.001 0 .001 0 .001];
```

```
a=.5; beta=40;
```

```
x = SolodeFrac(ynot ,T, a, beta);
```

```
t=1:T;
```

```
z = x;
```

```
z(:,5) = [];
```

```
createfigure1(z);
```

```
toc
```

```
%%%%%%%%%% Estimation
```

```
tic
```

```
global actual T ynot;
```

```
ynot = [1 -.001 0 .001 0 .001];
```

```
t=1:T;
```

```
actual=x(:,5);
```

```
a0=.1; beta0=20;
```

```
options=optimset('TolX',1e-40,'TolFun',1e-40,'Display','iter','  
↪ MaxIter',120,'MaxFunEvals',2000);%,'Jacobian','on');%,'  
↪ alg','interior-point');%,'GradObj','on','alg','interior-  
↪ point'
```

```
[phat SSEmin]=fminsearch(@ESS,[a0,beta0],options)
```

```
RSS=ESS(phat)/1000; %dlen=length(tspan);
```

```
dlen=T;
```

```
MLF=(1/(2*pi*RSS/dlen)^(dlen/2))*exp(-dlen/2);
```

```
sigma = sqrt(RSS/dlen);
```

```
q=length(phat)-3;
```

```
AICc = -2*log(MLF)+2*(q)+(2*q*(q+1)/(dlen-q-1));
```

```
BICc = -2*log(MLF)+q*log(dlen)+(2*q*(q+1)/(dlen-q-1));
```

```
y = SolodeFrac(ynot,T,phat(1),phat(2));
```

```
toc
```

```
t=1:T;
```

```
zy = y;
```

```
zy(:,5) = [];
```

```
createfigure1(z);
```

```
% Error
```

```
plot(t,x-actual,'LineWidth',2);  
xlabel('t','FontSize',12,'FontName','Times'); ylabel('Error','  
↪ FontSize',12,'FontName','Times');
```

```
createfigureError(x-y);
```

```
% sim of fitted
```

#### **solodeFrac.m**

```
function x = SolodeFrac(ynot,T,a,beta)  
x=zeros(0,1);  
for t=1:T  
    y=(t^a)/gamma(a+1); tey=100; te=tey*y;  
    xspan = linspace(0,y,1+te);  
    [X,Y] = ode45(@odeFrac2,xspan,ynot,[],t,a,beta);  
    x=[x;Y(end,:)];  
end
```

#### **odeFrac.m**

```
%ODE function
```

```
function xprime = odeFrac2(v,x,tt,a,beta)  
%% Auxillary functions  
% f=@(u,x)(u+x);  
% u=tt*(1-(1-(v)./((tt^a)/gamma(a+1))).^(1/a));
```

```
%% parameters
```

```
mu=(1/60);
```

```
delta=(365/7);
```

```
sigma=(365/21);
```

```
%% SEIR
```

```
xprime(1) = (mu.^a) - (beta.^a).*x(1).*x(3) - (mu.^a).*x(1);
```

```
↪ %S'
```

```
xprime(2) = (beta.^a).*x(1).*x(3) - (delta.^a).*x(2) - (mu.^a).*x(2)
```

```
↪ ; %E'
```

```
xprime(3) = (delta.^a).*x(2) - (mu.^a).*x(3) - (sigma.^a).*x(3);
```

```
↪ %I'
```

```
xprime(4) = (sigma.^a).*x(3) - (mu.^a).*x(4); %R'
```

```
xprime(5) = (delta.^a).*x(2); %C'
```

```
%% Return
```

```
xprime = xprime(:);
```

### ESS.m

```
function [E] = ESS(para)
```

```
global actual T ynot;
```

```
a=para(1);
```

```
beta=para(2);
```

```
ymodel=SolodeFrac(ynot,T,a,beta);
```

```
residd = ymodel(:,5)-actual;
```

```
E = residd.*residd;
```

```
E=sum(E)*1000;
```

## BIBLIOGRAPHY

- [1] A. CROEZE, L. PITTMAN, AND W. REYNOLDS, *Solving nonlinear least-squares problems with the gauss-newton and levenberg-marquardt methods*, 2012.
- [2] E. DEMIRCI AND N. OZALP, *A method for solving differential equations of fractional order*, *Journal of Computational and Applied Mathematics*, 236 (2012), pp. 2754–2762.
- [3] K. DIETHELM, *The analysis of fractional differential equations: An application-oriented exposition using differential operators of Caputo type*, Springer, 2010.
- [4] J. P. C. DOS SANTOS, L. C. CARDOSO, E. MONTEIRO, AND N. H. LEMES, *A fractional-order epidemic model for bovine babesiosis disease and tick populations*, in *Abstract and Applied Analysis*, vol. 2015, Hindawi Publishing Corporation, 2015.
- [5] M. ISHTEVA, *Properties and applications of the caputo fractional operator*, MSc. Thesis, (2005).
- [6] M. J. KEELING AND P. ROHANI, *Modeling infectious diseases in humans and animals*, Princeton University Press, 2008.
- [7] I. PODLUBNY, *Fractional differential equations: an introduction to fractional derivatives, fractional differential equations, to methods of their solution and some of their applications*, vol. 198 of *Mathematics in Science and Engineering*, Academic press, 1998.
- [8] I. PODLUBNY, *Geometric and physical interpretation of fractional integration and fractional differentiation*, arXiv preprint math/0110241, (2001).

## BIOGRAPHICAL SKETCH

Daniel Medina was born on September 20, 1991 and has one older brother. Graduated from University of Texas Pan American. He earned his masters degree in mathematics with a concentration of statistics at the University of Texas Rio Grande Valley. Daniel is also working on his teaching certificate with hopes to start teaching in the fall of 2017. He can be reached through email by contacting [dpmedin@gmail.com](mailto:dpmedin@gmail.com).